Int. J. Appl. Comput. Math (2025) 11:112
https://doi.org/10.1007/s40819-025-01928-4

ORIGINAL PAPER

A Mathematical Model of Pneumococcal Pneumonia Infection Dynamics Using Treatment and Vaccination Interventions

Zakirullah[1]

Accepted: 7 May 2025 / Published online: 26 May 2025

Abstract
This research focuses on pneumococcal pneumonia respiratory infection caused by *Streptococcus pneumoniae* bacteria by considering various epidemiological aspects. Researchers have discovered that elevating vaccination and hospitalization rates results in a decline in pneumococcal pneumonia disease cases. This study examines an epidemic model incorporating vaccination and treatment factors to conceptualize pneumococcal pneumonia transmission. A deterministic model with six compartments of pneumococcal pneumonia is built based on vaccinations and treatment to comprehend pneumococcal pneumonia infection spreads and preventative measures. In addition to the positivity, boundedness, existence, and uniqueness of the solution, the biologically viable region is established. The disease-free equilibrium point of global stability is illustrated by employing the Castillo-Chavez stability criterion, and its local stability analysis is demonstrated via the linearization approach, which leads to a result $R_0 < 1$. The next-generation matrix is utilised to calculate the basic reproduction number (R_0). Stability analysis via the Lyapunov function (LF) proves that the model of an endemic equilibrium is globally stable. Contour plots and 3D meshes are utilized to examine the impact of various parameters on (R_0). The trajectories of the state variables in the pneumococcal pneumonia model converge toward the equilibrium point. The Partial Rank Correlation Coefficient (PRCC) global technique examines parameter sensitivity. The pneumococcal pneumonia model is numerically solved using the Nonstandard Finite Difference (NSFD) to calculate the numerical results. In the NSFD numerical framework, a pneumococcal pneumonia dynamics model is simulated.

Keywords Pneumococcal pneumonia mathematical model · Sensitivity analysis · Stability analysis · Numerical simulations · Nonstandard finite difference

✉ Zakirullah
zakirullahbzt@gmail.com

[1] School of Mathematical Sciences, University of Electronic Science and Technology of China, Chengdu 611731, China

Introduction

According to reports, pneumonia is an infection caused by bacteria that affect the lungs. The respiratory system is impacted by pneumonia, a bacterial infection that typically begins in the upper respiratory tract and extends to the nervous system, middle ear, and bloodstream [1–3]. Children under the age of five are most commonly affected by pneumococcal pneumonia, and older individuals have a higher mortality rate. The likelihood of contracting pneumococcal pneumonia increases for individuals with pre-existing conditions such as liver disease, lung infection, chronic heart disease, and sickle cell disease. Additionally, the risk is elevated for those receiving anti-infective medications after an organ transplant or for HIV/AIDS patients. Viruses, bacteria, and fungi can all cause viral infections. Patients with throat or respiratory system infections are more likely to spread the bacterium. Infected individuals spread the disease by inhaling respiratory droplets. Many children carry bacteria in the throats without becoming ill. Chest pain, fast breathing, shortness of breath, coughing, headaches, and strong shaking chills are some of the symptoms of this disease [4–6].

Pneumonia prevention can be accomplished through environmental control measures, screening, immunizations, accurate diagnosis, and effective treatment of other infections [7]. Treatment and vaccination are the most effective methods of preventing viral pneumonia infections, and they are available for children and adults. The most commonly recommended vaccines are PCV (Pneumococcal conjugate vaccine) and PPV (Pneumococcal polysaccharide vaccine) [8]. For young and old, PPVs are necessary, whereas PCs are required for youngsters [9]. Treatment, diagnostic tools, and education are all necessary to prevent antibiotic resistance [10]. The majority of pneumonia patients start to exhibit clinical improvement 48–72 h after starting the right antibiotic treatment. The antibiotic amoxicillin is a good option for treating *S. pneumonia*, and hospitalization is recommended for severe cases of the disease. Depending on patient condition, beta-lactam antibiotics such as ceftriaxone or amoxicillin are frequently used as first-line therapy. Adjunctive treatments, such as anti-inflammatory drugs and oxygen supplements, can control respiratory complications. Targeted antimicrobial treatment improves results and reduces resistance when the causative pathogen is accurately identified using sputum culture or PCR. For severe presentations, hospitalisation is advised, especially when there is hypoxaemia, a changed mental state, or multilobar infiltration. Approximately 600,000 children are saved each year by antibiotic treatment, according to [11].

Vaccination and treatment reduce new cases and disease severity [12]. Vaccination against Haemophilus influenzae type b (Hib) and pneumococcal conjugate vaccine (PCV) targeting pneumococcus prevent childhood pneumonia. PCVs reduce the incidence of pneumococcal pneumonia in non-vaccinated individuals by reducing the nasopharyngeal transmission of vaccine-specific serotypes of *S. pneumoniae* [13]. Herd immunity occurs indirectly. This study aims to treat and vaccinate children with PCV against *S. pneumonia*. However, concerns including insufficient vaccination coverage and the rise of non-vaccine serotypes make continued monitoring and vaccine development necessary. It is still crucial to increase vaccination availability using integrated public health initiatives in order to maximise the impact on all populations. Most people recover from vaccinations easily and without complications. The majority experience only moderate, temporary side effects like weariness, low-grade fever, or injection site pain. As a result, vaccinations offer significant advantages that outweigh the minimal risks and serious side effects are rare. Long-term

complications are rare in immunocompromised patients, however recovery from moderate post-vaccination symptoms can be prolonged. For full recovery, supportive care which includes rest and hydration is usually sufficient. Furthermore, mathematical models can be used to develop or implement strategies for disease control, including understanding transmission phenomena, infection mechanisms, and epidemiological processes [14]. A compartmental mathematical model and vaccination strategies are presented in [15]. Recent developments in epidemiology have emphasized models that combine stochastic control, delay-induced dynamics, and fractional calculus in order to capture complex transmission patterns in infectious and noninfectious conditions [16–19]. A mathematical model is useful in determining disease potential severity and defining interventions to fight and control it [20, 21]. A compartmental mathematical model involving vaccination strategies for controlling infectious diseases has been considered in [22]. Greenhalgh et al. [23] and Lamb et al. [24] developed a model of pneumonia transmission among young children.

The paper is structured as follows: Section 1 provides an introduction and sets the groundwork for the research. Moving on to Sect. 2, the model formulation is detailed, encompassing the compartments of the pneumococcal pneumonic infection model and their respective parameter descriptions. Section 3 delves into the properties of the $\mathcal{SCIRVT}$ model, such as positivity, boundedness and conditions ensuring existence and uniqueness. Following this, Sect. 4 analyses, including the disease-free equilibrium point, basic reproduction number, stability, and sensitivity analysis. Section 5 is dedicated to the Nonstandard Finite Difference (NSFD) scheme for the pneumococcal pneumonia model model. In Sect. 6, the focus shifts to model simulation, which investigates the effects of different input factors on system dynamics. Finally, conclusion is drawn in Sect. 7.

Mathematical Model Formulation

In this paper section, epidemiological compartment models of infectious diseases for pneumococcal pneumonia transmission under the treatment and vaccination are constructed. The total human population $\mathcal{N}_h$ is classified into six compartments: susceptible $(\mathcal{S})$, carrier $(\mathcal{C})$, infected $(\mathcal{I})$, recovered $(\mathcal{R})$, vaccination $(\mathcal{V})$, and treatment $(\mathcal{T})$. The formulation assumes a natural mortality rate φ and a recruitment rate π. The vaccination rate for susceptible individuals is denoted by ν. In contrast, the vaccination rate for treated individuals is denoted by ϵ, while the pneumonia-treated individuals losing immunity τ. The recovery rate of the infected class is denoted by δ, while the recovery rate of the carrier class is indicated by κ. The treatment rate $\varkappa$ and the rate at which carrier individuals develop symptoms is represented by ω. The infection force, denoted by ρ, is detailed as follows: $\rho = \varpi(I + \beta C)$ where $\varpi = \theta\,\vartheta$, with ϑ representing the probability of infection, θ the contact rate, and ϖ the transmission rate. The following compartmental diagram (Fig. 1) explains the scenario well;

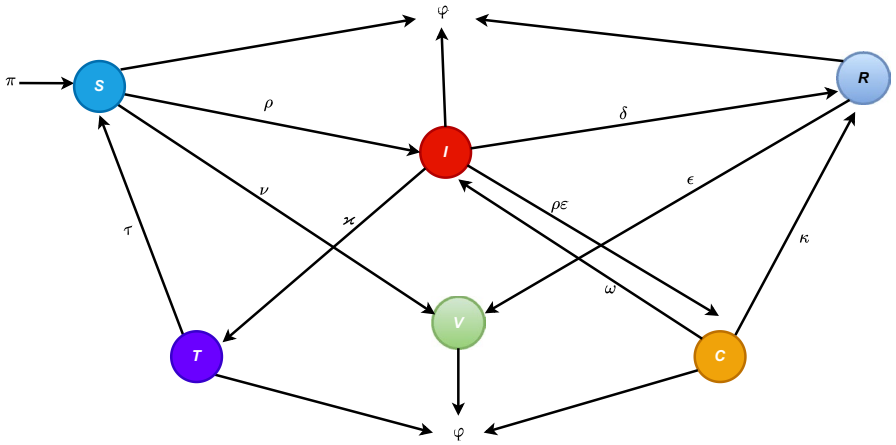

Fig. 1 Compartmental flow diagram illustrating the transmission dynamics of the pneumococcal pneumonia disease mathematical model

$$\begin{aligned}
\frac{d\mathcal{S}}{dt} &= \pi + \tau\mathcal{T} - (\rho + \nu + \varphi)\mathcal{S},\\
\frac{d\mathcal{C}}{dt} &= \rho\varepsilon\mathcal{S} - (\omega + \kappa + \varphi)\mathcal{C},\\
\frac{d\mathcal{I}}{dt} &= \rho(1-\varepsilon)\mathcal{S} + \omega\mathcal{C} - (\delta + \varkappa + \varphi)\mathcal{I},\\
\frac{d\mathcal{R}}{dt} &= \kappa\mathcal{C} + \delta\mathcal{I} - (\epsilon + \varphi)\mathcal{R},\\
\frac{d\mathcal{V}}{dt} &= \nu\mathcal{S} + \epsilon\mathcal{R} - \varphi\mathcal{V},\\
\frac{d\mathcal{T}}{dt} &= \varkappa\mathcal{I} - (\tau + \varphi)\mathcal{T}.
\end{aligned} \tag{1}$$

with the set of initial conditions

$\mathcal{S}(0) > 0, \mathcal{C}(0) \geq 0, \mathcal{I}(0) \geq 0, \mathcal{R}(0) \geq 0, \mathcal{V}(0) \geq 0, \mathcal{T}(0) \geq 0.$

Existence and Uniqueness

To verify the existence and uniqueness of the solution to model (1), rewrite it in the form form (2). This approach allows us to apply the conditions and techniques outlined in [25, 26] , thereby establishing the required properties

$$\frac{du}{dt} = g(t,u), u(t_0) = u_0. \tag{2}$$

Consider $u : R_+ \to R_6$ as a real-valued function represented by $u(t) = (\mathcal{S}(t), \mathcal{C}(t), \mathcal{I}(t), \mathcal{R}(t), \mathcal{V}(t), \mathcal{T}(t))$ with $u(0) = \mathcal{S}(0), \mathcal{C}(0), \mathcal{I}(0), \mathcal{R}(0), \mathcal{V}(0), \mathcal{T}(0))$ as the initial vector. The function $g(t, u)$ is defined as follows.

$$g(t,u) = \begin{pmatrix} g_1(t,u) \\ g_2(t,u) \\ g_3(t,u) \\ g_4(t,u) \\ g_5(t,u) \\ g_6(t,u) \end{pmatrix} = \begin{pmatrix} \pi + \tau\mathcal{T} - (\rho + \nu + \varphi)\mathcal{S} \\ \rho\varepsilon\mathcal{S} - (\omega + \kappa + \varphi)\mathcal{C} \\ \rho(1-\varepsilon)\mathcal{S} + \omega\mathcal{C} - (\delta + \varkappa + \varphi)\mathcal{I} \\ \kappa\mathcal{C} + \delta\mathcal{I} - (\epsilon + \varphi)\mathcal{R} \\ \nu\mathcal{S} + \epsilon\mathcal{R} - \varphi\mathcal{V} \\ \varkappa\mathcal{I} - (\tau + \varphi)\mathcal{T} \end{pmatrix}$$

The column vector resides in R_+^6, with its components aligned with the right-hand side of system (1). The existence and uniqueness of solutions to system (1) are ensured by the theorems provided.

Theorem 3.1 *Let $\mathcal{D} \subseteq R^n$, and suppose $g : \mathcal{D} \to R^n$ is continuously differentiable. Then, on any convex, compact subset $\mathcal{D} \subseteq R^n$ the mapping g fulfills the Lipschitz condition.*

$$\|g(t,u_1) - g(t,u_2)\| \leq c\,\|u_1 - u_2\|\,, \tag{3}$$

With a Lipchitz constant $c > 0$. Here, c represents the supremum of the derivative of g on $\mathcal{D}$, expressed as for a Lipschitz constant $c \succ 0$. where k is defined as the supremum of the derivative of g over $\mathcal{D}$, written as:

$$k = \sup_{y \in D} \left| \frac{dg}{dy} \right|$$

condition (3) is fulfilled by ensuring that the partial derivatives

$$\left\{ \frac{\partial g_i}{\partial u_i} \right\}_{i,j=1,2,3,\ldots,n}$$

is continuous and bounded in $\mathcal{D}$.

Condition (3) holds when the partial derivatives of $\left\{ \frac{\partial g_i}{\partial u_i} \right\}_{i,j=1,2,3,\ldots,n}$ are continuous and bounded in $\mathcal{D}$.

Theorem 3.2 *If g(t, u) has continuous partial derivatives $\frac{\partial g_i}{\partial u_i}$ over a bounded, closed, and convex set R in R, then then it will satisfy a Lipschitz condition within R.*

Theorem 3.3 *Let $\mathcal{D} = \{|t - t_0| \prec a, |u - u_0| \leq b, \quad u = (u_1, u_2, u_3, ..., u_n), u_0 = (u_{10}, u_{20}, u_{30}, ..., u_{n0})\}$ represent the domain. Assuming g(t, u) satisfies the Lipschitz condition (3) when both (t, u_1) and (t, u_2) lie in D, then system (2) has unique continuous vector solution u(t) in the interval $|t - t_0| \leq a$, where a is a positive constant.*

Theorem 3.4 *Let $\mathcal{D}$ be the domain defined in 3.3, where condition (3) and the result from Theorm 3.2 are both satisfied. In such a case, system (1) has a solution that remains bounded within D.*

Proof The partial derivatives $\frac{\partial g_i}{\partial u_i}$, for i,j$\in \{1, 2, ..., 6\}$ satisfy both continuity and boundedness. To verify this, the partial derivatives in the equations of model (2) as detailed below:

$$\frac{\partial g_1}{\partial \mathcal{S}} = -(\rho+\nu+\varphi)\mathcal{S}, \left|\frac{\partial g_1}{\partial \mathcal{S}}\right| = |-(\rho+\nu+\varphi)\mathcal{S}| \prec \infty,$$
$$\frac{\partial g_1}{\partial \mathcal{C}} = -\varpi\beta\mathcal{S}, \left|\frac{\partial g_1}{\partial \mathcal{C}}\right| = |-\varpi\beta\mathcal{S}| \prec \infty,$$
$$\frac{\partial g_1}{\partial \mathcal{I}} = -\varpi\mathcal{S}, \left|\frac{\partial g_1}{\partial \mathcal{I}}\right| = |-\varpi\mathcal{S}| \prec \infty,$$
$$\frac{\partial g_1}{\partial \mathcal{R}} = 0, \left|\frac{\partial g_1}{\partial \mathcal{R}}\right| = |0| \prec \infty,$$
$$\frac{\partial g_1}{\partial \mathcal{V}} = 0, \left|\frac{\partial g_1}{\partial \mathcal{V}}\right| = |0| \prec \infty,$$
$$\frac{\partial g_1}{\partial \mathcal{T}} = \tau, \left|\frac{\partial g_1}{\partial \mathcal{T}}\right| = |\tau| \prec \infty.$$

The partial derivatives for g_2, g_3, g_4, g_5 and g_5 follow the same steps as g_1. Since the partial derivatives are continuous and bounded, Theorem 3.3, guarantees the existence of a unique solution to system (1) in the region $\mathcal{D}$. □

Properties of the Model

This subsection discusses the positive analysis and boundness of the model (1).

Model Positivity Analysis

All state variables must be non-negative for model (1) to be epidemiologically meaningful.

Theorem 3.5 *The region* $\Omega_+ = \{(\mathcal{S},\mathcal{C},\mathcal{I},\mathcal{R},\mathcal{V},\mathcal{T})(t); (\mathcal{S} > 0, \mathcal{C} \geq 0, \mathcal{I} \geq 0, \mathcal{R} \geq 0, \mathcal{V} \geq 0, \mathcal{T} \geq 0)\}$ *is a positive invariant for model (1).*

Proof Suppose that $(\mathcal{S},\mathcal{C},\mathcal{I},\mathcal{R},\mathcal{V},\mathcal{T})$ is solution of (1), the first equation of the system (1) can be written as follows:

$$\frac{d\mathcal{S}}{dt} = \pi + \tau T - (\rho+\nu+\varphi)\mathcal{S} \geq -(\rho+\nu+\varphi)\mathcal{S}.$$

This implies,

$$\frac{d\mathcal{S}}{dt} \geq -(\rho+\nu+\varphi)\mathcal{S}.$$

By separating variables,

$$\int_{S(0)}^{\mathcal{S}(t)} \frac{dS}{\mathcal{S}} \geq \int_0^t (\rho+\nu+\varphi)dt.$$

Thus,

$$\begin{array}{c} \mathcal{S}(t) \geq \mathcal{S}(0) exp^{-(\rho+\nu+\varphi)t}, \\ \mathcal{S}(0) \geq 0, \forall t > 0. \end{array} \tag{4}$$

Hence the region Ω_+ is a positive invariant and the solution of model (1) will remain inside Ω_+. The remaining equations can be solved with same method: $\mathcal{C}(0) \geq 0, \mathcal{I}(0) \geq 0, \mathcal{R}(0) \geq 0, \mathcal{V}(0) \geq 0, \mathcal{T}(0) \geq 0$. Then the solutions $\mathcal{S}(t), \mathcal{C}(t), \mathcal{I}(t), \mathcal{R}(t), \mathcal{V}(t), \mathcal{T}(t)$ of the model are positive $\forall t > 0$. □

Bounded Region for the Proposed Model

This subsection discusses the boundness of the model (1). Utilize the following theorem to get the bounded feasible region for the proposed model (1).

Theorem 3.6 *The feasible solution set $\Omega \subseteq R^6$ of the model (1) with initial conditions $\mathcal{S} \geq 0, \mathcal{C} \geq 0, \mathcal{I} \geq 0, \mathcal{R} \geq 0, \mathcal{V} \geq 0, \mathcal{T} \geq 0$ forms a positive invariant set, guaranteeing that all trajectories originating within this set will remain in biologically feasible regions over time.*

Proof Add all equations of model (1), where

$$\mathcal{N}_h(t) = (\mathcal{S} + \mathcal{C} + \mathcal{I} + \mathcal{R} + \mathcal{V} + \mathcal{T})(t). \tag{5}$$

In the next step, differentiate the equation with respect to time t to obtain

$$\frac{d\mathcal{N}_h}{dt} = \frac{d\mathcal{S}}{dt} + \frac{d\mathcal{C}}{dt} + \frac{d\mathcal{I}}{dt} + \frac{d\mathcal{R}}{dt} + \frac{d\mathcal{V}}{dt} + \frac{d\mathcal{T}}{dt}. \tag{6}$$

Substituting model (1) equations yields equation (7)

$$\begin{array}{l} \dfrac{d\mathcal{N}_h}{dt} = \pi + \tau\mathcal{T} - \rho\mathcal{S} - \nu\mathcal{S} - \varphi\mathcal{S} + \rho\varepsilon\mathcal{S} - \omega\mathcal{C} \\ \qquad - \kappa\mathcal{C} - \varphi\mathcal{C} + \rho\mathcal{S} - \rho\varepsilon\mathcal{S} + \omega\mathcal{C} - \delta\mathcal{I} - \varkappa\mathcal{I}. \end{array} \tag{7}$$

Therefore, simplify Eq. (7) further yield

$$\frac{d\mathcal{N}_h}{dt} = \pi - (\mathcal{I} + \mathcal{S} + \mathcal{C} + \mathcal{R} + \mathcal{V} + \mathcal{T})\varphi,$$

where,

$$\begin{array}{l} \mathcal{I} + \mathcal{S} + \mathcal{C} + \mathcal{R} + \mathcal{V} + \mathcal{T} = \mathcal{N}_h, \\ \dfrac{d\mathcal{N}_h}{dt} \leq \pi - \mathcal{N}_h\varphi \Longleftrightarrow \dfrac{d\mathcal{N}_h}{dt} + \mathcal{N}_h\varphi \leq \pi. \end{array} \tag{8}$$

Equation (8) can be calculated using a separable method,

$$\int_{\mathcal{N}_h(0)}^{\mathcal{N}_h(t)} \frac{d\mathcal{N}_h}{\pi - \mathcal{N}_h\varphi} \leq \int_0^t dt,$$

This implies,

$$\mathcal{N}_h(t) \leq \frac{\pi}{\varphi}(1 - \exp^{-\varphi t}) + \mathcal{N}_h(0)\exp^{-\varphi t},$$

at $t \to \infty$,

$$\mathcal{N}_h(\infty) \leq \frac{\pi}{\varphi}.$$

It can be seen in Eq. (9) that the $\mathcal{SCIRVT}$ model (1) is biologically and epidemiologically meaningful. Solution of the system exists in R_+^6, thus a biologically feasible region is constructed as follows:

$$\Omega = (\mathcal{S}, \mathcal{C}, \mathcal{I}, \mathcal{R}, \mathcal{V}, \mathcal{T}) \in R_+^6 : 0 \leq \mathcal{N}_h(t) \leq \frac{\pi}{\varphi}. \tag{9}$$

All terms are positive in model (1), so the solution is bounded. □

Analysis of the Model

This section discusses disease-free equilibrium, reproduction numbers, the local stability of DFE, and its global stability.

Disease Free Equilibrium Point E_0

$$\frac{d\mathcal{S}}{dt} = \frac{d\mathcal{C}}{dt} = \frac{d\mathcal{I}}{dt} = \frac{d\mathcal{R}}{dt} = \frac{d\mathcal{V}}{dt} = \frac{d\mathcal{T}}{dt} = 0.$$

Thus, the disease-free equilibrium points for System (1) are expressed as

$$E_0 = \left(\frac{\pi}{\rho + \nu + \varphi}, 0, 0, 0, \frac{\nu\pi}{\varphi(\rho + \nu + \varphi)}, 0\right). \tag{10}$$

Basic Reproduction Number (R_0)

The basic reproduction number (R_0) is the average number of cases generated by a single infected individual throughout the infection period [34]. If $R_0 < 1$, the disease will fade

out of the population. Conversely, if $R_0 > 1$, the disease will persist or spread within the population. R_0 denotes the basic reproduction number is the dominant (largest) eigenvalue (spectral radius) of the matrix $FV^{-1} = [\frac{\partial F_i}{\partial x}(E_0)]\text{and}V = [\frac{\partial V_i}{\partial x}(E_0)]$.

Let $y = (\mathcal{C}, \mathcal{I}, \mathcal{T})$. The model can be expressed as follows:

$$\frac{dy}{dt} = F - V. \tag{11}$$

where $F = F^- - F^+$. Here, V represents the rate at which new infections appear in the compartments, F^+ refers to the rate at which individuals are transferred into the compartment, and F^- represents the rate at which individuals leave the compartment. In this context

$$F = \begin{pmatrix} \varpi\beta\varepsilon\mathcal{S} & \varpi\varepsilon\mathcal{S} & 0 \\ \varpi\beta(1-\varepsilon)\mathcal{S} & \varpi(1-\varepsilon)\mathcal{S} & 0 \\ 0 & 0 & 0 \end{pmatrix},$$

and the transition matrix as

$$V = \begin{pmatrix} k_1 & -\varkappa & 0 \\ -\omega & k_2 & 0 \\ 0 & 0 & k_3 \end{pmatrix},$$

where,

$$\begin{aligned} k_1 &= \omega + \kappa + \varphi, \\ k_2 &= \delta + \varkappa + \varphi, \\ k_3 &= \tau + \varphi. \end{aligned}$$

The inverse of V is

$$V^{-1} = \begin{pmatrix} \frac{k_2}{-\varkappa\omega + k_1 k_2} & \frac{\varkappa}{-\varkappa\omega + k_1 k_2} & 0 \\ \frac{\omega}{-\varkappa\omega + k_1 k_2} & \frac{k_1}{-\varkappa\omega + k_1 k_2} & 0 \\ 0 & 0 & \frac{1}{k_3} \end{pmatrix}.$$

The next generation matrix is of the form

$$FV^{-1} = \begin{pmatrix} l_1 & l_2 & 0 \\ l_3 & l_4 & 0 \\ 0 & 0 & 0 \end{pmatrix}, \tag{12}$$

where,

$$
\begin{aligned}
l_1 &= \mathcal{S}_0\varpi\omega\frac{\varepsilon}{-\varkappa\omega+k_1k_2}+\mathcal{S}_0\varpi\beta\varepsilon\frac{k_2}{-\varkappa\omega+k_1k_2},\\
l_2 &= \mathcal{S}_0\varkappa\varpi\beta\frac{\varepsilon}{-\varkappa\omega+k_1k_2}+\mathcal{S}_0\varpi\varepsilon\frac{k_1}{-\varkappa\omega+k_1k_2},\\
l_3 &= \mathcal{S}_0\varpi\frac{\omega}{-\varkappa\omega+k_1k_2}(-\varepsilon+1)+\mathcal{S}_0\varpi\beta\frac{k_2}{-\varkappa\omega+k_1k_2}(-\varepsilon+1),\\
l_4 &= \mathcal{S}_0\varkappa\varpi\frac{\beta}{-\varkappa\omega+k_1k_2}(-\varepsilon+1)+\mathcal{S}\varpi\frac{k_1}{-\varkappa\omega+k_1k_2}(-\varepsilon+1).
\end{aligned}
$$

The eigenvalues of matric (12) are given as

$$
\left\{0,0,\mathcal{S}_0\varpi\frac{\varkappa\beta\varepsilon+\varepsilon k_1-\varkappa\beta-k_1-\omega\varepsilon-\beta\varepsilon k_2}{\varkappa\omega-k_1k_2}\right\},
$$

Reproduction number R_0(dominant eigenvalue) is the basic reproduction number.

$$
R_0=\frac{\pi\varpi(\varkappa\beta\varepsilon+\varepsilon k_1-\varkappa\beta-k_1-\omega\varepsilon-\beta\varepsilon k_2)}{(\rho+\nu+\varphi)(\varkappa\omega-k_1k_2)}.
$$

Stability Analysis

This subsection discusses local and global stability.

Local Stability of the Disease-Free Equilibrium (DFE)

Theorem 4.1 *In system (1), the disease-free equilibrium E_0 is local asymptotically stable if $R_0 < 1$, otherwise it is unstable.*

Proof The Jacobian matrix for the system (1) is shown below at E_0

$$
J(E_0)=\begin{pmatrix}
-(\rho+\nu+\varphi) & 0 & 0 & 0 & 0 & \tau\\
\rho\varepsilon & -(\omega+\kappa+\varphi) & 0 & 0 & 0 & 0\\
\rho(1-\varepsilon) & 0 & -(\delta+\varkappa+\varphi) & 0 & 0 & 0\\
0 & \kappa & \delta & -(\omega+\varphi) & 0 & 0\\
\nu & 0 & 0 & \omega & -\varphi & 0\\
0 & 0 & \varkappa & 0 & 0 & -(\tau+\varphi)
\end{pmatrix}. \quad (13)
$$

Now, at the disease-free equilibrium: $E_0=(\frac{\pi}{\rho+\nu+\varphi},0,0,0,\frac{\nu\pi}{\varphi(\rho+\nu+\varphi)},0)$. The Jacobian matrix (13) at disease-free equilibrium E_0 gives

$$
J(E_0)=\begin{pmatrix}
-(\nu+\varphi) & 0 & 0 & 0 & 0 & \tau\\
0 & -k1 & 0 & 0 & 0 & 0\\
0 & 0 & -k2 & 0 & 0 & 0\\
0 & \kappa & \delta & -(\epsilon+\varphi) & 0 & 0\\
\nu & 0 & 0 & \omega & -\varphi & 0\\
0 & 0 & \varkappa & 0 & 0 & -k_3
\end{pmatrix}, \quad (14)
$$

where,

$$
\begin{aligned}
k_1 &= \omega + \kappa + \varphi, \\
k_2 &= \delta + \varkappa + \varphi, \\
k_3 &= \tau + \varphi.
\end{aligned}
$$

The stability of the disease-free equilibrium requires trace $J(E_0) < 0$ and the $\det J(E_0) > 0$. As a result, from the Jacobian matrix (14), we can see that

$$
\begin{aligned}
J(E_0) &= -[(\nu + \varphi) + k_1 + k_2 + (\epsilon + \varphi) + \varphi + k_3] < 0, \\
\det J(E_0) &= 2k^2\varphi\nu\epsilon k_3 + 2k^2\varphi^3 k_3 + 2k^2\varphi^2\nu k_3 + 2k^2\varphi^2\epsilon k_3 > 0.
\end{aligned}
$$

Asymptotically, the model (1) is locally stable under treatment and vaccination interventions. The fact that the $J(E_0) < 0$ and the trace $\det J(E_0) > 0$ proves this. □

Global Stability of the Disease-Free Equilibrium

In this subsection, the two conditions, $\mathcal{C}_1$ and $\mathcal{C}_2$, guarantee global asymptotically stable E_0. Based on [35] approach to proving the global stability of the disease-free equilibrium point, system (1) as follows

$$
\begin{aligned}
\frac{d\mathcal{X}}{dt} &= A(\mathcal{X}, \mathcal{Y}), \\
\frac{d\mathcal{Y}}{dt} &= B(\mathcal{X}, \mathcal{Y}), \mathcal{B}(\mathcal{X}, 0) = 0
\end{aligned}
$$

In this context, $\mathcal{X} = (\mathcal{S}, \mathcal{R}, \mathcal{V})$ represents the uninfected compartments, and $\mathcal{Y} = (\mathcal{C}, \mathcal{I}, \mathcal{T})$ represents the infected compartments. If $R_0 < 1$ is met by the two conditions, then the E_0 is globally asymptotically stable.

$$
\mathcal{C}_1 : \frac{d\mathcal{X}}{dt} = A(\mathcal{X}_0, 0), \tag{15}
$$

$\mathcal{X}_0$ is asymptotically global under condition $\mathcal{C}_1$.

$$
\mathcal{C}_2 : \frac{d\mathcal{Y}}{dt} = \frac{\partial \mathcal{B}}{\partial \mathcal{Y}}(\mathcal{X}_0, 0)\mathcal{Y} - \hat{\mathcal{B}}(\mathcal{X}, \mathcal{Y}), \hat{\mathcal{B}}(\mathcal{X}, \mathcal{Y}) \geq 0 \tag{16}
$$

Theorem 4.2 *Global asymptotic stability of the disease-free equilibrium point $E_0 = (\mathcal{X}_0, 0)$ is ensured if the three Castillo-Chavez criterion conditions are satisfied.*

Proof Proving the global asymptotic stability of the disease-free equilibrium point is to identify $\mathcal{A}(\mathcal{X}, \mathcal{Y})$ and $\mathcal{B}(\mathcal{X}, \mathcal{Y})$. □

In light of our model Eq. (1)

$$
\mathcal{A}(\mathcal{X}, \mathcal{Y}) = \begin{cases} \pi + \tau\mathcal{T} - (\rho + \nu + \varphi)\mathcal{S}, \\ \nu\mathcal{S} + \epsilon\mathcal{R} - \varphi\mathcal{V}, \\ \kappa\mathcal{C} + \delta\mathcal{I} - (\epsilon + \varphi)\mathcal{R}, \end{cases} \tag{17}
$$

and

$$\mathcal{B}(\mathcal{X},\mathcal{Y}) = \begin{cases} \rho\varepsilon\mathcal{S} - (\omega+\kappa+\varphi)\mathcal{C}, \\ \rho(1-\varepsilon)\mathcal{S} + \omega\mathcal{C} - (\delta+\varkappa+\varphi)\mathcal{I}, \\ \varkappa\mathcal{I} - (\tau+\varphi)\mathcal{T}. \end{cases}$$

As shown in Theorem 4.1, the first condition is already proven.

Now,

$$(\mathcal{S}_0, \mathcal{V}_0, \mathcal{T}_0) \to \left(\frac{\pi}{\rho+\nu+\varphi}, \frac{\nu\pi}{\varphi(\rho+\nu+\varphi)}, 0\right).$$

Addressing the second condition of the Castillo-Chavez criterion for the reduced system. From the first equation in system (17). The following equation emerges:

$$\begin{aligned} \frac{d\mathcal{S}}{dt} =& \pi + \tau\mathcal{T} - (\rho+\nu+\varphi)\mathcal{S}, \\ \frac{d\mathcal{S}}{dt} +& (\rho+\nu+\varphi)\mathcal{S} = \pi + \tau\mathcal{T}_0, \\ S =& \frac{(\pi+\tau\mathcal{T}_0)}{(\rho+\nu+\varphi)} + ce^{-(\rho+\nu+\varphi)t}, \end{aligned}$$

Since $t \to \infty,\ e^{-(\rho+\nu+\varphi)t} \to 0,\ S \to \frac{\pi}{\rho+\nu+\varphi} = S_0$.

Following this approach, we can compute the rest of the equations. As a result, the second condition of the Castillo-Chavez criterion holds. Lastly, we must show the third criterion as indicated below:

Condition is defined by $\mathcal{C}_2$ if $\frac{\partial\mathcal{B}}{\partial\mathcal{Y}} = \mathcal{B}(\mathcal{X}_0, 0)$ is M-matrix and $\hat{\mathcal{B}}(\mathcal{X},\mathcal{Y}) \geq 0$ for $(\mathcal{X},\mathcal{Y}) \in \mathcal{D}$.

Now,

$$\frac{\partial\mathcal{B}}{\partial\mathcal{Y}} = \mathcal{B}(\mathcal{X}_0, 0) = \begin{pmatrix} \beta\varepsilon\mathcal{S} - (\omega+\kappa+\varphi) & \varpi\varepsilon\mathcal{S} & 0 \\ \beta(1-\varepsilon)\mathcal{S} + \omega & \varpi(1-\varepsilon)\mathcal{S} - (\delta+\varkappa+\varphi) & 0 \\ 0 & \varkappa & -(\tau+\varphi) \end{pmatrix}$$

Since the off-diagonal entries are non-negative, it follows that $\frac{\partial\mathcal{B}}{\partial\mathcal{Y}}\ (\mathcal{X}_0, 0)$ is an M-matrix.

The result can be derived from Eq. (16) as follows

$$\hat{\mathcal{B}}(\mathcal{X},\mathcal{Y}) = \begin{pmatrix} (\mathcal{N}_h - \mathcal{S})\,\rho \\ 0 \\ 0 \end{pmatrix}.$$

Therefore, $\mathcal{N}_h \geq \mathcal{S} \geq 0$, can conclude that $\hat{B}(X,Y) \geq 0$. Thus, the diseases free equilibrium is stable globally.

Global Stability of Endemic Equilibrium Point

The Lyapunov method determines the global stability of the endemic equilibrium point E_* [36, 37]. Considering the theorem and its proof, the LF is obtained.

Theorem 4.3 *The endemic equilibrium point E_* is globally asymptotically stable when $R_0 > 1$; otherwise, it becomes unstable.*

Proof The global stability of the endemic equilibrium point, we apply the Lyapunov function, which is defined as

$$L(x_i, ..., x_n) = \sum_{i=1}^{n} \frac{1}{2} \left[x_i - x_i^*\right]^2,$$

Assuming that n is the number of compartments, x_i represents the disease-free equilibrium compartments, and x_i^* indicates the endemic compartments.

$$\begin{aligned} L(\mathcal{S}, \mathcal{C}, \mathcal{I}, \mathcal{R}, \mathcal{V}, \mathcal{T}) = \frac{1}{2}[(\mathcal{S} - \mathcal{S}^*) + (\mathcal{C} - \mathcal{C}^*) + (\mathcal{I} - \mathcal{I}^*) \\ + (\mathcal{R} - \mathcal{R}^*) + (\mathcal{V} - \mathcal{V}^*) + (\mathcal{T} - \mathcal{T}^*)]^2. \end{aligned} \tag{18}$$

The following solution is obtained by taking the derivative of function L with respect to time t

$$\begin{aligned} L' = [(\mathcal{S} + \mathcal{C} + \mathcal{I} + \mathcal{R} + \mathcal{V} + \mathcal{T} - (\mathcal{S}^* + \mathcal{C}^* + \mathcal{I}^* + \mathcal{R}^* + \mathcal{V}^* + \mathcal{T}^*)] \\ \left(\frac{d\mathcal{S}}{dt} + \frac{d\mathcal{C}}{dt} + \frac{d\mathcal{I}}{dt} + \frac{d\mathcal{R}}{dt} + \frac{d\mathcal{V}}{dt} + \frac{d\mathcal{T}}{dt}\right). \end{aligned} \tag{19}$$

Equation (6) gives

$$\frac{d\mathcal{N}_h}{dt} = \frac{d}{dt}(\mathcal{S} + \mathcal{C} + \mathcal{I} + \mathcal{R} + \mathcal{V} + \mathcal{T}).$$

As a result Eq. (8).

$$\frac{d\mathcal{N}_h}{dt} = \pi - \mathcal{N}_h\varphi. \tag{20}$$

But from Eq. (7) given that

$$(\mathcal{S}^* + \mathcal{C}^* + \mathcal{I}^* + \mathcal{R}^* + \mathcal{V}^* + \mathcal{T}^*) \leq \frac{\pi}{\varphi}. \tag{21}$$

Substituting Eqs. (20) and (21) into Eq. (19),

$$L' = \left(\mathcal{N}_h - \frac{\pi}{\varphi}\right)(\pi - \mathcal{N}_h\varphi). \tag{22}$$

Equation (22) is given with a simplified form.

$$L' = -\tfrac{1}{\varphi}(\varphi - \mathcal{N}_h\pi)^2. \tag{23}$$

□

$L' < 0$ is a strictly Lyapunov function as presented in (23) which shows that the endemic equilibrium point is globally asymptotically stable when $R_0 > 1$ in the region Ω. According to Eq. (23), L is a strictly LF, so the endemic equilibrium point is globally asymptotically stable when $R_0 > 1$. L' converges in the positive region as $t \to \infty$, and $L' = 0$ if and only if set $\mathcal{S} = \mathcal{S}^*, \mathcal{C} = \mathcal{C}^*, \mathcal{I} = \mathcal{I}^*, \mathcal{R} = \mathcal{R}^*, \mathcal{V} = \mathcal{V}^*, \mathcal{T} = \mathcal{T}^*$.

Sensitivity Analysis

To perform sensitivity analysis, the concept of standard methods, such as the Partial Rank Correlation Coefficient (PRCC), is used for sensitivity analysis to find the most significant parameters in the model. The sensitivity of R_0 with respect to a parameter X is calculated as follows:

$$\Gamma_X^{R_0} = \frac{\partial R_0}{\partial X} \times \frac{X}{R_0} \tag{24}$$

$$\Gamma_\nu^{R_0} = -\frac{\nu}{k_4} < 0, \tag{25}$$

The sensitivity indicex of R_0 to parameter ρ, β, ε, π, ϖ and θ can be calculated as using definition (24)

$$\begin{aligned}
\Gamma_\rho^{R_0} &= -\frac{\rho}{k_4} < 0,\\
\Gamma_\beta^{R_0} &= \frac{\beta(\varkappa + \delta\varepsilon + \varepsilon\varphi)}{k_1 + \beta\varkappa - \kappa\varepsilon - \varepsilon\varphi + \beta\delta\varepsilon + \beta\varepsilon\varphi} > 0,\\
\Gamma_\varepsilon^{R_0} &= -\frac{\varepsilon\left(\kappa + \varphi - \beta\delta - \beta\varphi\right)}{k_1 + \beta\varkappa - \kappa\varepsilon - \varepsilon\varphi + \beta\delta\varepsilon + \beta\varepsilon\varphi} < 0,\\
\Gamma_\pi^{R_0} &= \frac{\alpha\varpi k_4\left(\varkappa\omega - k_1k_2\right)\left(k_1 + \beta\varkappa + \varepsilon\omega - \varepsilon k_1 - \beta\varkappa\varepsilon + \beta\varepsilon k_2\right)}{\alpha\varpi k_4\left(\varkappa\omega - k_1k_2\right)\left(k_1 + \beta\varkappa + \varepsilon\omega - \varepsilon k_1 - \beta\varkappa\varepsilon + \beta\varepsilon k_2\right)} = 1,\\
\Gamma_\varpi^{R_0} &= \frac{\alpha\varpi k_4\left(\varkappa\omega - k_1k_2\right)\left(k_1 + \beta\varkappa + \varepsilon\omega - \varepsilon k_1 - \beta\varkappa\varepsilon + \beta\varepsilon k_2\right)}{\alpha\varpi k_4\left(\varkappa\omega - k_1k_2\right)\left(k_1 + \beta\varkappa + \varepsilon\omega - \varepsilon k_1 - \beta\varkappa\varepsilon + \beta\varepsilon k_2\right)} = 1,\\
\Gamma_\theta^{R_0} &= \frac{\theta\alpha\varpi k_4\left(\varkappa\omega - k_1k_2\right)\left(k_1 + \beta\varkappa + \varepsilon\omega - \varepsilon k_1 - \beta\varkappa\varepsilon + \beta\varepsilon k_2\right)}{\theta\alpha\varpi k_4\left(\varkappa\omega - k_1k_2\right)\left(k_1 + \beta\varkappa + \varepsilon\omega - \varepsilon k_1 - \beta\varkappa\varepsilon + \beta\varepsilon k_2\right)} = 1,
\end{aligned} \tag{26}$$

Using definition the sensitivity indices of R_0 w.r.t $\vartheta, \delta, \kappa, \varphi, \omega$ and $\varkappa$ can be compute as

$$\begin{aligned}
\Gamma_{\vartheta}^{R_0} &= \frac{\theta\alpha\vartheta k_4\left(\varkappa\omega - k_1k_2\right)\left(k_1 + \beta\varkappa + \varepsilon\omega - \varepsilon k_1 - \beta\varkappa\varepsilon + \beta\varepsilon k_2\right)}{\theta\alpha\vartheta k_4\left(\varkappa\omega - k_1k_2\right)\left(k_1 + \beta\varkappa + \varepsilon\omega - \varepsilon k_1 - \beta\varkappa\varepsilon + \beta\varepsilon k_2\right)} = 1,\\
\Gamma_{\delta}^{R_0} &= \frac{\delta\left(k_1 + \beta\varkappa\right)\left(\kappa\varepsilon - k_1 + \varepsilon\varphi\right)}{\left(\varphi^2 + k_1\varphi + \delta\omega + \kappa k_2\right)\left(k_1 + \beta\varkappa - \varepsilon(\kappa + \varphi) + \beta\varepsilon(\delta + \varphi)\right)} < 0,\\
\Gamma_{\kappa}^{R_0} &= -\frac{\kappa\left(\omega + \beta k_2\right)\left(\varkappa + \delta\varepsilon + \varepsilon\varphi\right)}{\left(\varphi^2 + \delta\omega + \kappa k_2 + \varphi k_1\right)\left(k_1 + \beta\varkappa - \varepsilon^2\varphi + \beta\delta\varepsilon - \kappa\varepsilon\varphi + \beta\varepsilon\varphi\right)} < 0,\\
\Gamma_{\varphi}^{R_0} &= \frac{\varphi k_4(\beta\varepsilon - \varepsilon + 1) - \varphi(k_4 + 1)(k_1 + \beta\varkappa + \varepsilon\omega - \varepsilon k_1 - \beta\varkappa\varepsilon + \beta\varepsilon k_2)}{k_4(k_1 + \beta\varkappa + \varepsilon\omega - \varepsilon k_1 - \beta\varkappa\varepsilon + \beta\varepsilon k_2)} < 0,\\
\Gamma_{\omega}^{R_0} &= \frac{\omega\left(\varkappa + \delta\varepsilon + \varepsilon\varphi\right)\left(\kappa + \varphi - \beta\delta - \beta\varphi\right)}{\left(\varphi^2 + \delta\omega + \kappa k_2 + \varphi k_1\right)\left(k_1 + \beta\varkappa - \varepsilon^2\varphi + \beta\delta\varepsilon - \kappa\varepsilon\varphi + \beta\varepsilon\varphi\right)} > 0,\\
\Gamma_{\varkappa}^{R_0} &= \frac{\varkappa\left(\kappa\varepsilon - k_1 + \varepsilon\varphi\right)\left(\kappa + \varphi - \beta\delta - \beta\varphi\right)}{\left(\varphi^2 + k_2\varphi + \delta\omega + \kappa k_2\right)\left(k_1 + \beta\varkappa - \kappa\varepsilon - \varepsilon\varphi + \beta\delta\varepsilon + \beta\varepsilon\varphi\right)} < 0,
\end{aligned} \tag{27}$$

in this context,

$$\begin{aligned}
k_1 &= \omega + \kappa + \varphi,\\
k_2 &= \delta + \varkappa + \varphi,\\
k_3 &= \tau + \varphi,\\
k_4 &= \nu + \rho + \varphi.
\end{aligned}$$

The sensitivity indices Eqs. (25)–(27) need a clearer mathematical framework, making it difficult to understand how parameter values affect reproduction numbers. Using Table 1 in Eqs. (25)–(27) yields numerical values, resulting in a sensitivity index of 1 for the pneumonia recruitment rate. Increased pneumonia recruitment rates increase R_0 values. This implies increased recruitment leads to a higher disease transmission rate and more infections.

Two parameters emerged as having the most negative sensitivities. The first parameter ν is the vaccination rate for susceptible humans. Due to its strong negative sensitivity of -0.68241, it implies that increasing the vaccination rate would result in a lower disease transmission rate or a reduced number of infections. Similarly, the second parameter, $\varkappa$ associated with treatment rate, exhibits a negative sensitivity of -0.57868, suggesting that increasing the treatment rate would decrease the disease impact. In other words, higher vaccination and treatment rates would reduce the spread or severity of the infection. After substituting the values Table 1, get the sensitivity indices Table 2.

Construction of New Schemes

In this section, Nonstandard Finite Difference (NSFD) approaches can capture the nonlinear behavior of pneumococcal pneumonia infection. These schemes are based on a step-wise approximation function $\Theta(h) = 1 - \exp^{-h}$, which is a real-valued function [38, 39]. The function $\Theta(h)$satisfies the condition $\Theta(h) \to 0$ as $h \to 0$.

By applying this method to Eq. (1) yields the following system

Table 1 Input parameter with description and values for numerical simulations

Parameter	Description	Initial Value	Source
β	Transmission coeffcient for the carrier subgroup	0.001124/day	[27]
θ	Rate of contact	1–10/day	[27]
δ	Recovery rate of the infected class	0.0714/day	Assumed
κ	Recovery rate of the carrier class	0.0115/day	Assumed
ϑ	Probability for a contact to cause infection	0.89−0.99/day	[27]
ω	Rate of symptom development for carriers	0.01096/day	[28]
ϵ	Vaccination rate for treated individuals	0.338/day	[29]
φ	Natural mortality rate	0.0002/day	[30]
π	Recruitment rate	10.09/day	[31]
ν	Vaccination rate for susceptible humans	0.0621/day	[31]
$\varkappa$	Treatment rate of pneumonia	0.2/day	[32, 33]
τ	Pneumonia treated individuals waning immunity	0.13/day	Assumed
ρ	Force of infection of susceptible individuals	0.0287/day	[31]
ε	Fraction of susceptible individuals that join the carriers	0.338/day	Assumed
ϖ	Transmission rate	7.6/day	Assumed

Table 2 Numerical values of sensitivity indices

Parameter symbols	Sensitivity Index	Parameter symbols	Sensitivity Index
π	1.00000	φ	−0.01006
ϖ	1.00000	ε	−0.20716
θ	1.00000	ρ	−0.31538
ϑ	1.00000	κ	−0.38666
β	0.01329	δ	−0.40688
ω	0.38009	$\varkappa$	−0.57868
		ν	−0.68241

$$\begin{aligned}
\frac{\mathcal{S}^{m+1}-\mathcal{S}^{m}}{\Theta(h)} =&\pi+\tau\mathcal{T}^{m+1}-(\rho+\nu+\varphi)\mathcal{S}^{m+1},\\
\frac{\mathcal{C}^{m+1}-\mathcal{C}^{m}}{\Theta(h)} =&\rho\varepsilon\mathcal{S}^{m+1}-(\omega+\kappa+\varphi)\mathcal{C}^{m+1},\\
\frac{\mathcal{I}^{m+1}-\mathcal{I}^{m}}{\Theta(h)} =&\rho(1-\varepsilon)\mathcal{S}^{m+1}+\omega\mathcal{C}^{m+1}-(\delta+\varkappa+\varphi)\mathcal{I}^{m+1},\\
\frac{\mathcal{R}^{m+1}-\mathcal{R}^{m}}{\Theta(h)} =&\kappa\mathcal{C}^{m+1}+\delta\mathcal{I}^{m+1}-(\epsilon+\varphi)\mathcal{R}^{m+1},\\
\frac{\mathcal{V}^{m+1}-\mathcal{V}^{m}}{\Theta(h)} =&\nu\mathcal{S}^{m+1}+\epsilon\mathcal{R}^{m+1}-\varphi\mathcal{V}^{m+1},\\
\frac{\mathcal{T}^{m+1}-\mathcal{T}^{m}}{\Theta(h)} =&\varkappa\mathcal{I}^{m+1}-(\tau+\varphi)\mathcal{T}^{m+1}.
\end{aligned} \tag{28}$$

Simplifying system (28) and setting $1-\Theta(h)=\exp^{-h}$,the following result is obtained

$$S^{m+1}=\frac{\mathcal{S}^{m}+(\pi+\tau\mathcal{T}^{m+1})\exp^{-h}}{1+k_4\exp^{-h}}, \tag{29}$$

$$\mathcal{C}^{m+1}=\frac{\mathcal{C}^{m}+\rho\varepsilon\exp^{-h}\mathcal{S}^{m+1}}{1+k_1\exp^{-h}}, \tag{30}$$

$$\mathcal{I}^{m+1}=\frac{\mathcal{I}^{m}+(\rho(1-\varepsilon)\mathcal{S}^{m+1}+\omega\mathcal{C}^{m+1})\exp^{-h}}{1+k_2\exp^{-h}}, \tag{31}$$

$$\mathcal{R}^{m+1}=\frac{\mathcal{R}^{m}+(\kappa\mathcal{C}^{m+1}+\delta\mathcal{I}^{m+1})\exp^{-h}}{1+(\epsilon+\varphi)\exp^{-h}}, \tag{32}$$

$$\mathcal{V}^{m+1}=\frac{\mathcal{V}^{m}+(\nu\mathcal{S}^{m+1}+\epsilon\mathcal{R}^{m+1})\exp^{-h}}{1+\varphi\exp^{-h}}, \tag{33}$$

$$\mathcal{T}^{m+1}=\frac{\mathcal{T}^{m}+\varkappa\exp^{-h}\mathcal{I}^{m+1}}{1+k_3\exp^{-h}}. \tag{34}$$

Study of the Scheme

Theorem 5.1 *Numerical interpretation of the system dynamics within the biological domain Ω of the continuous model (1) is carried out using the NSFD scheme (29)–(34).*

Proof Initially, Eq. (8) are taken into account and discretized in the following way:

$$\frac{d\mathcal{N}_h}{dt}=\pi-\mathcal{N}_h\varphi. \tag{35}$$

The discretized form of the system of Eqs. (35) is now expressed as follows:

$$\frac{\mathcal{N}_h^{m+1}-\mathcal{N}_h^m}{\Theta(h)}=\pi-\mathcal{N}_h^{m+1}\varphi. \tag{36}$$

Equations (29)–(34) are used to determine the condition of positivity in the NSFD scheme. Setting $1-\Theta(h)=\exp^{-h}$ in Eq. (36) yields:

$$\mathcal{N}_h^{m+1}=\frac{\pi(1-\exp^{-h})}{(1+\varphi(1-\exp^{-h})}+\frac{N^m}{(1+\varphi(1-\exp^{-h})}. \tag{37}$$

As presented, the system of Eqs. (29)–(34) is not yet in a computationally convenient form. By substituting Eq. (34) into the Eq. (29) of the system, leads to the following result

$$\begin{aligned}S^{m+1}&(1-\frac{\exp^{-2h}\,\tau\varkappa\rho(\varepsilon-k_1\exp^{-h}-\varepsilon\omega+\varepsilon k_1\exp^{-h}-1)}{(k_4\exp^{-h}+1)\,(k_3\exp^{-h}+1)\,(k_2k_4\exp^{-h}+1)\,(k_1\exp^{-h}+1)})\\&=\frac{1}{k_4\exp^{-h}+1}\left(\pi\exp^{-h}+\mathcal{S}^m\right)\\&\quad+\tau\frac{\mathcal{T}^m(1+k_1\exp^{-h}+k_2\exp^{-h}+k_1k_2\exp^{-2h})+\varkappa\omega\exp^{-h}\mathcal{C}^m+a\mathcal{I}^m(\varkappa+a\varkappa k_1)}{(k_1\varkappa\omega\exp^{-h}+1)\,(k_2\varkappa\omega\exp^{-h}+1)\,(k_3\varkappa\omega\exp^{-h}+1)\,(k_4\varkappa\omega\exp^{-h}+1)},\end{aligned} \tag{38}$$

to keep the calculations manageable, we set

$$K_1=\frac{\exp^{-2h}\,\tau\varkappa\rho(\varepsilon-k_1\exp^{-h}-\varepsilon\omega+\varepsilon k_1\exp^{-h}-1)}{(k_4\exp^{-h}+1)\,(k_3\exp^{-h}+1)\,(k_2k_4\exp^{-h}+1)\,(k_1\exp^{-h}+1)}\ ,$$

and

$$K_2=\ \tau\frac{\mathcal{T}^m(1+k_1\exp^{-h}+k_2\exp^{-h}+k_1k_2\exp^{-2h})+\varkappa\omega\exp^{-h}\mathcal{C}^m+a\mathcal{I}^m(\varkappa+a\varkappa k_1)}{(k_1\varkappa\omega\exp^{-h}+1)\,(k_2\varkappa\omega\exp^{-h}+1)\,(k_3\varkappa\omega\exp^{-h}+1)\,(k_4\varkappa\omega\exp^{-h}+1)}.$$

So that Eq. (38) can be written as

$$\mathcal{S}^{m+1}=\frac{1}{K_1\,(k_4\exp^{-h}+1)}\mathcal{S}^m+\frac{K_2+(\pi+K_2k_4)\exp^{-h}}{K_1\,(k_4\exp^{-h}+1)}. \tag{39}$$

Substituting Eq. (38) into Eq. (30) yields the following result

$$\mathcal{C}^{m+1}=\frac{1}{k_1\exp^{-h}+1}\mathcal{C}^m+\frac{\varepsilon\rho\exp^{-h}}{K_1\,(k_4\exp^{-h}+1)}\mathcal{S}^m+\frac{\varepsilon\rho\left(K_2+\pi\exp^{-h}+k_4\exp^{-h}K_2\right)\exp^{-h}}{K_1\,(k_4\exp^{-h}+1)}. \tag{40}$$

When Eqs. (38) and (40) are substituted into Eq. (31), the result is as follows

$$\begin{aligned}\mathcal{I}^{m+1}=&\frac{(1+k_1k_4)}{(k_1\exp^{-h}+1)\,(k_2\exp^{-h}+1)}\mathcal{I}^m+\frac{\omega(1+ak_2)}{(k_1\exp^{-h}+1)\,(k_2\exp^{-h}+1)}\mathcal{C}^m\\&+\frac{\rho\left(-\varepsilon+\varepsilon\omega\exp^{-h}+1\right)(K_2+\pi\exp^{-h}+\mathcal{S}^m+k_4\exp^{-h}K_2)\exp^{-h}}{K_1\,(k_4\exp^{-h}+1)}.\end{aligned} \tag{41}$$

The substitution of Eqs. (40) and Eq. (41) into Eq. (32) leads to the following result

$$\begin{aligned}\mathcal{R}^{m+1} =& \frac{(1+k_1\exp^{-h}+k_2\exp^{-h}+k_1k_2\exp^{-2h})}{(a\epsilon+a\varphi+1)(ak_1+1)(ak_2+1)}\mathcal{R}^m \\ &+ \frac{(\kappa+k_2\kappa\exp^{-h}+\delta\omega\exp^{-h})}{(\epsilon\exp^{-h}+\varphi\exp^{-h}+1)(k_1\exp^{-h}+1)(k_2\exp^{-h}+1)}\mathcal{C}^m \\ &+ \frac{(\delta+a\delta k_1)\exp^{-h}}{(\epsilon\exp^{-h}+\varphi\exp^{-h}+1)(k_1\exp^{-h}+1)(k_2\exp^{-h}+1)}\mathcal{I}^m \\ &+ \frac{\rho\left(\delta+\kappa\varepsilon-\delta\varepsilon+\delta\varepsilon\omega+\kappa\varepsilon k_2\exp^{-h}\right)(K_2+\pi\exp^{-h}+\mathcal{S}^m+K_2k_4\exp^{-h})\exp^{-2h}}{K_1(k_4\exp^{-h}+1)(k_2\exp^{-h}+1)(\epsilon\exp^{-h}+\varphi\exp^{-h}+1)}.\end{aligned} \tag{42}$$

Plugging Eq. (38) into Eq. (42) into Eq. (33) leads to the following outcome.

$$\begin{aligned}\mathcal{V}^{m+1} =& \frac{\mathcal{V}^m}{1+\varphi\exp^{-h}} + \frac{\nu(K_2+\pi\exp^{-h}+S^m+K_2k_4\exp^{-h})\exp^{-h}}{K_1(ak_4+1)} \\ &+ \frac{\epsilon(1+k_1\exp^{-h}+k_2\exp^{-h}+k_1k_2\exp^{-h})\exp^{-h}}{(\epsilon\exp^{-h}+\varphi\exp^{-h}+1)(k_1\exp^{-h}+1)(k_2\exp^{-h}+1)}\mathcal{R}^m \\ &+ \frac{\epsilon(\kappa+\kappa k_2\exp^{-h}+\delta\omega)\exp^{-h}}{(\epsilon\exp^{-h}+\varphi\exp^{-h}+1)(k_1\exp^{-h}+1)(k_2\exp^{-h}+1)}\mathcal{C}^m \\ &+ \frac{(\delta+a\delta k_1)\exp^{-h}}{(\epsilon\mathcal{I}^m+\varphi\mathcal{I}^m+1)(k_1\mathcal{I}^m+1)(k_2\mathcal{I}^m+1)}\mathcal{I}^m \\ &+ \frac{\epsilon\rho(\delta+\kappa\varepsilon-\delta\varepsilon+\delta\varepsilon\omega+a\kappa\varepsilon k_2)(K_2+\pi a+\mathcal{S}^m+aK_2k_4)\exp^{-3h}}{K_1(k_4\exp^{-h}+1)(k_2\exp^{-h}+1)(\epsilon\exp^{-h}+\varphi\exp^{-h}+1)}.\end{aligned} \tag{43}$$

Substituting Eq. (31) into Eq. (34) yields this result

$$\begin{aligned}\mathcal{T}^{m+1} =& \frac{1}{1+k_3\exp^{-h}}\mathcal{T}^m + \frac{\varkappa(1+k_1k_4)\exp^{-h}}{(k_1\exp^{-h}+1)(k_2\exp^{-h}+1)(1+k_3\exp^{-h})}\mathcal{I}^m \\ &+ \frac{\omega\varkappa(1+ak_2)\exp^{-h}}{(k_1\exp^{-h}+1)(k_2\exp^{-h}+1)(1+k_3\exp^{-h})}\mathcal{C}^m \\ &+ \frac{\rho\varkappa\left(-\varepsilon+\varepsilon\omega\exp^{-h}+1\right)(K_2+\pi\exp^{-h}+\mathcal{S}^m+k_4\exp^{-h}K_2)\exp^{-2h}}{K_1(k_4\exp^{-h}+1)(1+k_3\exp^{-h})}.\end{aligned} \tag{44}$$

Hence, $\mathcal{S}^m, \mathcal{C}^m, \mathcal{I}^m, \mathcal{R}^m, \mathcal{V}^m, \mathcal{T}^m$ are linear in $\mathcal{S}^{m+1}, \mathcal{C}^{m+1}, \mathcal{I}^{m+1}, \mathcal{R}^{m+1}, \mathcal{V}^{m+1}, \mathcal{T}^{m+1}$. Now, consider the system of Eqs. (39)–(44), where the right-hand side remains positive for all $m > 0$ and for any step size $h > 0$. Notably, the general NSFD scheme Eqs. (39)–(44) of model (1) imposes no restrictions on the step size h, making it a powerful method as discussed in [40,41]. The NSFD scheme is notable in that the variables $\mathcal{S}^{m+1}, \mathcal{C}^{m+1}, \mathcal{I}^{m+1}, \mathcal{R}^{m+1}, \mathcal{V}^{m+1}, \mathcal{T}^{m+1}$ in model (1) are entirely determined by the set $\mathcal{S}^m, \mathcal{C}^m, \mathcal{I}^m, \mathcal{R}^m, \mathcal{V}^m, \mathcal{T}^m$, using a step size h and non-negative parameters specified in Table 1. The structure of the denominator function does not require any specific or predefined form and is explicitly constructed. Additionally, the scheme guarantees that the solution remains positive for all values of the step size h. □

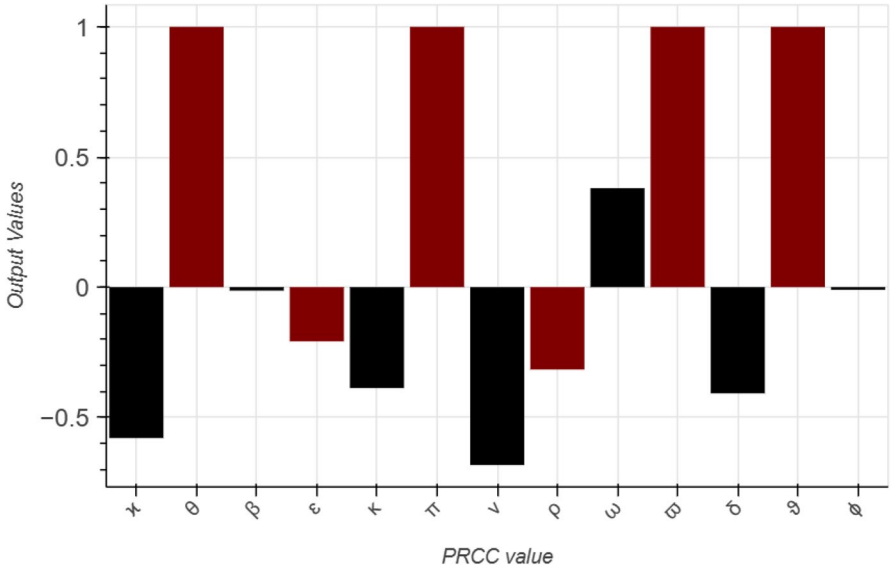

Fig. 2 Sensitivity test results for significance of input factors in R_0

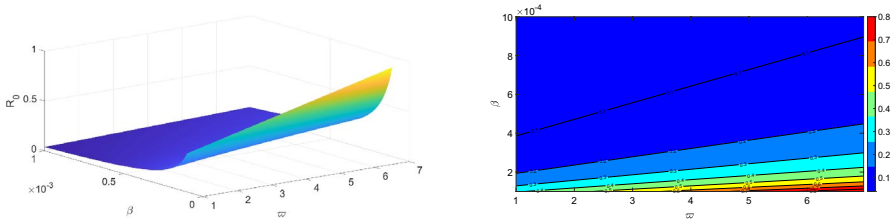

(a) (b)

Fig. 3 The subplot (**a**) depicts the effect of β(transmission coefficient for the carrier subgroup) and ϖ(transmission rate) on R_0, while (**b**) features the corresponding contour plot

Numerical Simulation

This section presents the numerical results for system (1). The pneumococcal pneumonia model is simulated using the NSFD method with the initial conditions set as $\mathcal{S}(0) = 300$, $\mathcal{C}(0) = 120, \mathcal{I}(0) = 100$, $R(0) = 70$, $\mathcal{V}(0) = 50$ and $\mathcal{T}(0) = 20$. The parameter values are taken from Table 1.

In Fig.2, illustrates the PRCC results for (R_0), depicting the sensitivity of (R_0) to various parameters in the model, which helps identify the most influential factors in pneumococcal pneumonia disease transmission. In Figs. 3, 4, 5, 6, 7, and 8, depicts the impact of these parameters on (R_0) using 3D mesh and contour plots, illustrating the visual representation of how changes in parameter values affect the basic reproduction number (R_0) across different scenarios. Figure 3 depicts the effect of the transmission coefficient for the carrier subgroup (β) and the transmission rate (ϖ) on R_0. The two parameters exhibit positive relationships with R_0, suggesting that increasing either enhances the spread of

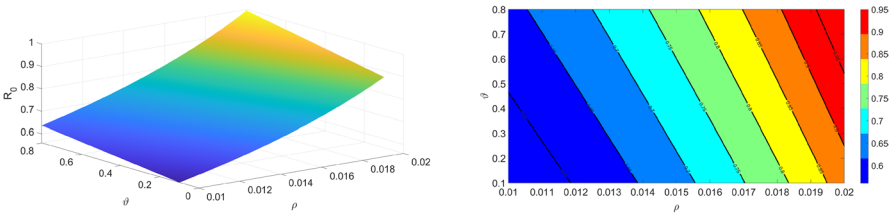

(a) **(b)**

Fig. 4 The subplot (**a**) depicts the effect of ϑ(probability for a contact to cause infection) and ρ(force of infection of susceptible individuals) on R_0, while (**b**) features the corresponding contour plot

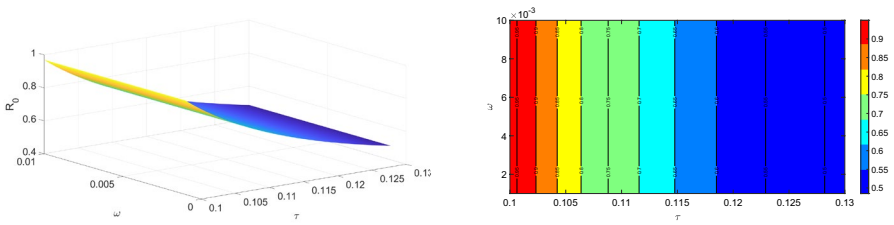

(a) **(b)**

Fig. 5 The subplot (**a**) depicts the effect of ω(rate of symptom development for carriers) and τ(pneumonia treated individuals losing Immunity) on R_0, while (**b**) features the corresponding contour plot

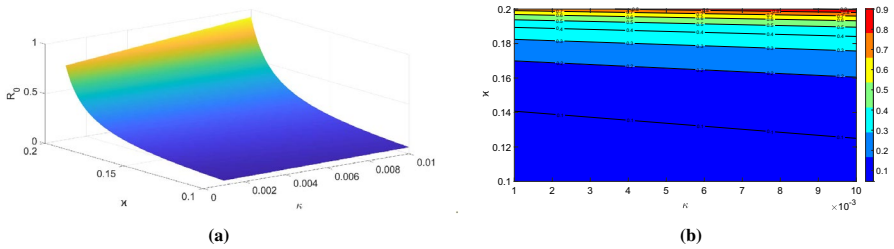

(a) **(b)**

Fig. 6 The subplot (**a**) depicts the effect of $\varkappa$(treatment rate of pneumonia) and κ(recovery rate of the carrier class) on R_0, while (**b**) features the corresponding contour plot

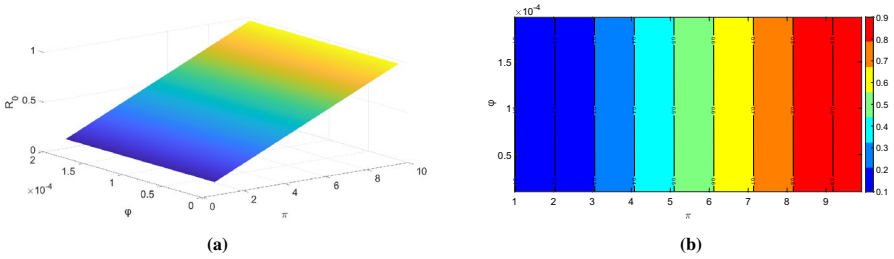

(a) **(b)**

Fig. 7 The subplot (**a**) depicts the effect of φ(natural mortality rate) and π(recruitment rate) on R_0, while (**b**) features the corresponding contour plot

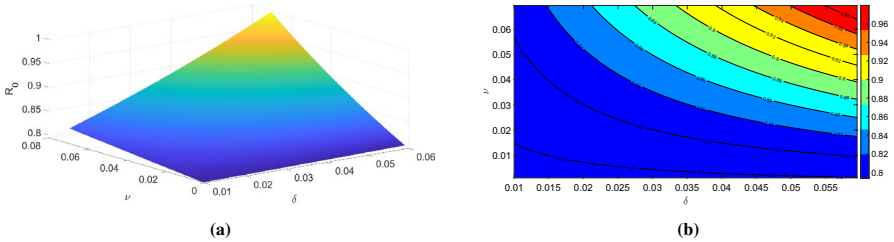

Fig. 8 The subplot (**a**) depicts the effect of ν(vaccination rate) and δ(recovery rate of the infected class) on R_0, while (**b**) features the corresponding contour plot

infection. The following figure, Fig. 4 in the same section examines the probability of infection upon contact (ϑ) and the force of infection experienced by susceptible individuals (ρ). Both these parameters have a positive impact on R_0, signifying the likelihood and intensity of disease transmission. Figure 5, the rate at which carriers develop symptoms (ω) and the rate at which treated individuals lose immunity (τ) are analyzed. An increase in ω leads to reduce R_0 by facilitating early detection and isolation, whereas a higher τ increasesR_0 by returning recovered individuals to the susceptible population more effectively. Figure 6, illustrates the relationship between the treatment rate of pneumococcal pneumonia $(\varkappa)$ and the recovery rate of the carrier class (κ) with R_0. Both parameters are negatively correlated with R_0, as faster treatment and quicker recovery reduce the duration of infectiousness, as a result limiting transmission. Figure 7 depicts the impact of the natural mortality rate (φ) and the recruitment rate (π) on R_0. Higher natural mortality rates reduce R_0 by reducing the number of individuals available to transmit the infection, in contrast to a higher recruitment rate, which introduces more susceptible individuals into the population, increasing R_0. Furthermore, Fig. 8, illustrates the effect of the vaccination rate (ν) and the recovery rate of the infected class (δ) on R_0. Higher values of ν and δ lead to a decline in R_0 by reducing the number of susceptible and infectious hosts, respectively, thus reducing disease spreading. In Fig. 9, illustrates the dynamics of the susceptible, carrier, infected, recovered, vaccination, and treatment classes over a period of 120 days. In Fig. 10, presents the force of infection (ρ) for varying values of 0.1230287, 0.2340257, 0.3450237, and 0.6780227, depicting the direct correlation between the infection rate and the impact on these classes. In Fig. 11, increasing the vaccination rate (ν) to 0.0601, 0.0606, 0.0609, and 0.0621 is shown to reduce the infection rate dramatically. Similarly, in Fig. 12, the treatment rate $(\varkappa)$ at 0.211, 0.232, 0.253, and 0.264 also demonstrates a reduction in the infection rate of pneumococcal pneumonia infection, highlighting the significance of vaccination efforts. These findings indicate that the vaccination rate significantly impacts the pneumococcal pneumonia model, while the treatment rate has a lesser effect. By increasing the vaccination rate, the dynamics of pneumococcal pneumonia are significantly reduced, effectively controlling the spread of pneumococcal pneumonia. In Figs. 13, 14, 15, display the endemic equilibrium originating from distinct origins, allowing insight into the dynamics of these classes under varying initial scenarios that converge toward the equilibrium point.

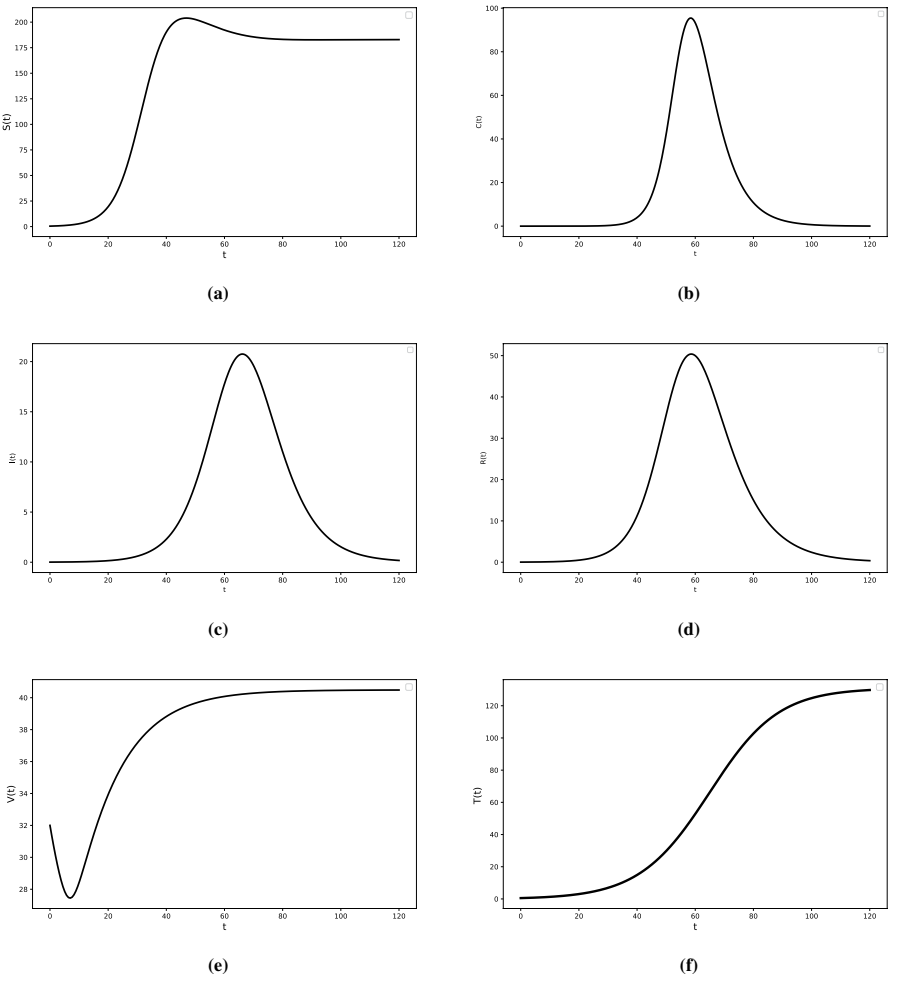

Fig. 9 The subfigures (**a**)–(**f**) present profiles for susceptible ($\mathcal{S}$), carrier ($\mathcal{C}$), infected ($\mathcal{I}$), recovered ($\mathcal{R}$), vaccination (V) and treatment (T) classes

Conclusion

This manuscript explores the transmission dynamics of pneumococcal pneumonia infection by incorporating key factors of treatment and vaccination within a mathematical compartmental model. The analysis covered various aspects, including the disease-free equilibrium point, positivity, feasible region, basic reproduction number, stability, and sensitivity of the proposed model. When $R_0 < 1$, the disease-free equilibrium (E_0) is stable, ensuring local and global stability. Conversely, when $R_0 > 1$, the disease-free equilibrium (E_0) becomes unstable. PRCC technique illustrates the importance of various input factors that can significantly influence pneumococcal pneumonia infection control. Pneumococcal pneumonia infection behaviour can be explained more accurately and precisely by fractional-order dynamics. Major factors influencing the spread of pneumococcal pneumonia in the popula-

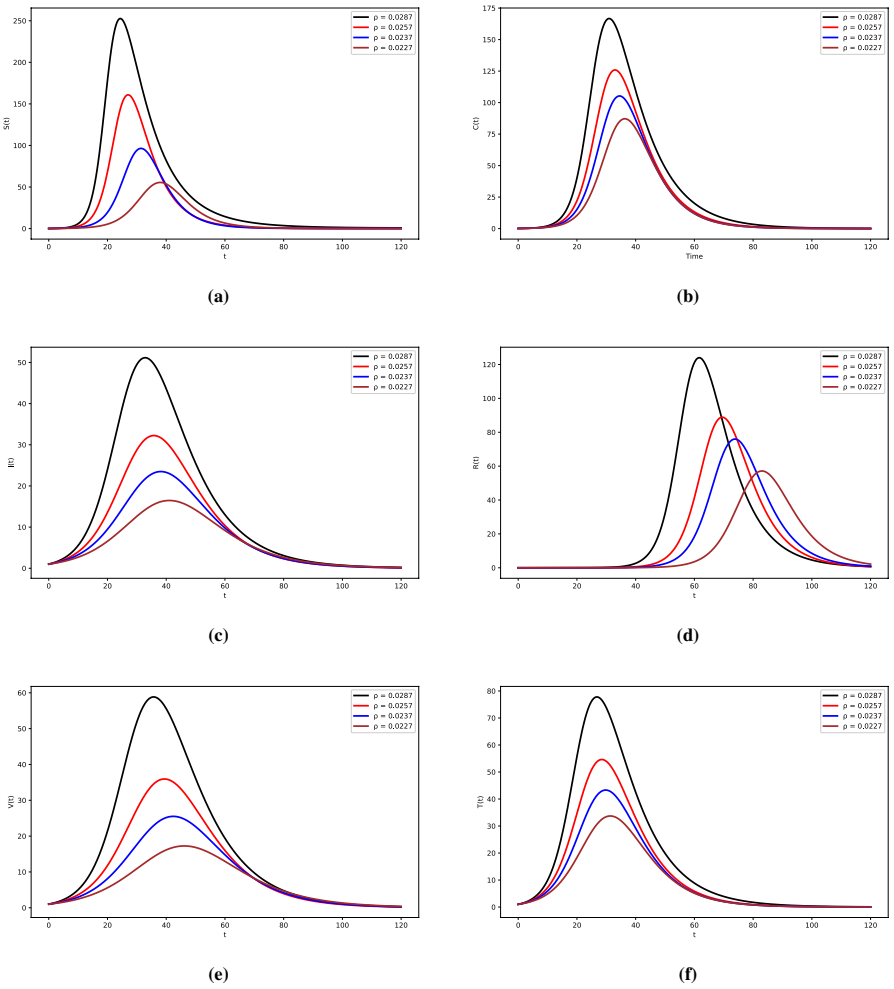

Fig. 10 The impact of the force of infection on the susceptible ($\mathcal{S}$), carrier ($\mathcal{C}$), infected ($\mathcal{I}$), recovered (R), vaccination ($\mathcal{V}$), and treatment($\mathcal{T}$) classes are depicted in subfigures (**a**)–(**f**), with ρ values of 0.0287, 0.0257, 0.0237 and 0.0227

tion include the transmission coefficient, force of infection, and probability of contact. However, the disease is controlled by rates of recovery, vaccination, treatment. Increasing the treatment and vaccination rates reduced the number of infected individuals. These findings show that strategically increasing treatment and vaccination rates and careful adjustments in model parameters can significantly influence the spread of pneumococcal pneumonia infection.

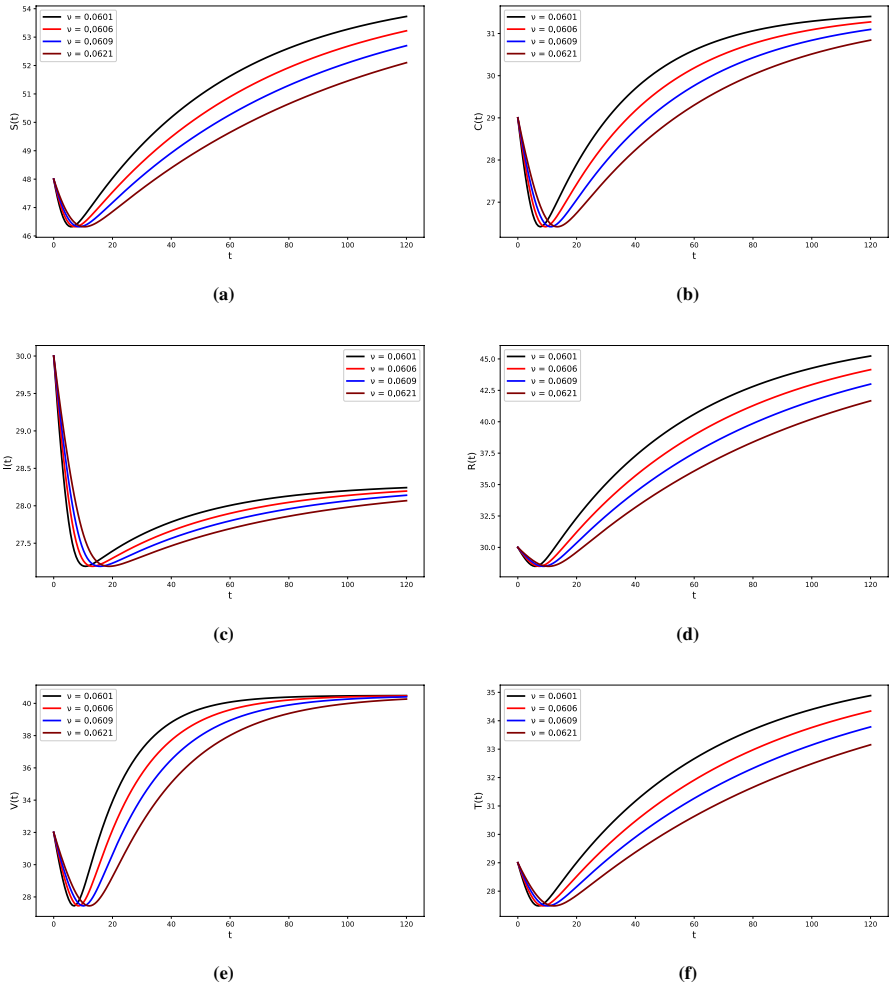

Fig. 11 The impact of the vaccination rate on the susceptible ($\mathcal{S}$), carrier ($\mathcal{C}$), infected ($\mathcal{I}$), recovered ($\mathcal{R}$), vaccination ($\mathcal{V}$), and treatment($\mathcal{T}$) classes are depicted in subfigures (**a**)–(**f**), with ν values of 0.0601, 0.0606, 0.0609 and 0.0621

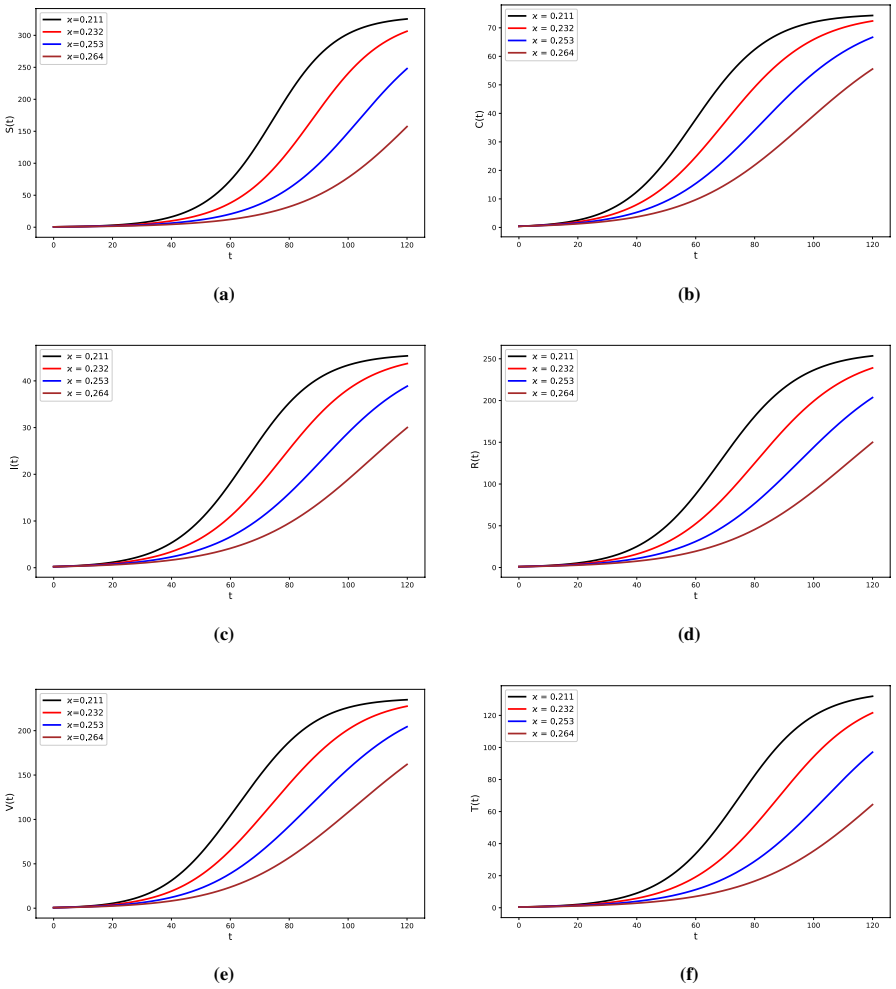

Fig. 12 The impact of the treatment rate on the susceptible ($\mathcal{S}$), carrier ($\mathcal{C}$), infected ($\mathcal{I}$), recovered ($\mathcal{R}$), vaccination ($\mathcal{V}$), and treatment($\mathcal{T}$) classes are depicted in subfigures (**a**)–(**f**), with $\varkappa$ values of 0.211, 0.232, 0.252 and 0.264

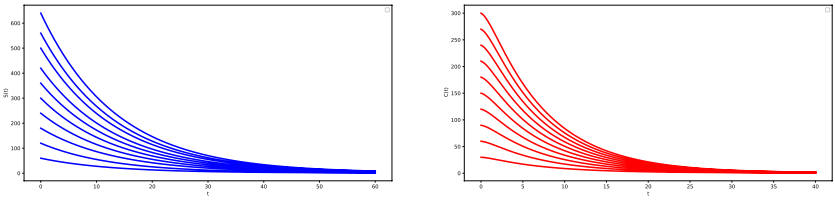

Fig. 13 Profile for the endemic equilibrium of susceptible and carrier individuals from distinct initial conditions

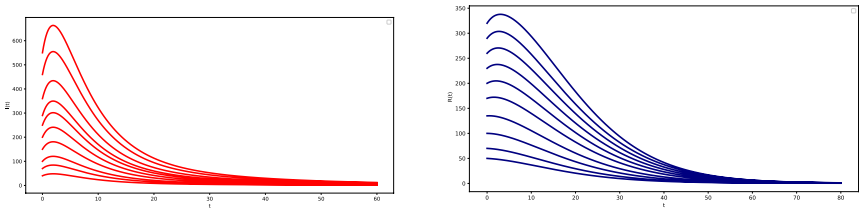

Fig. 14 Profile for the endemic equilibrium of infected and recovered individuals from distinct initial conditions

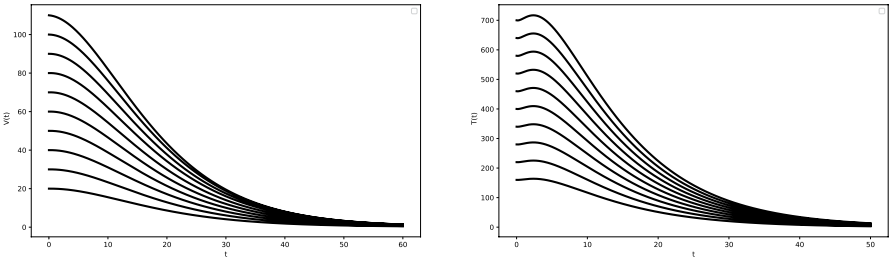

Fig. 15 Profile for the endemic equilibrium of vaccination and treatment of individuals from distinct initial conditions

Author Contributions Zakirullah: conceptualization, methodology, software, writing—reviewing and editing.

Funding This research received no external funding.

Data Availability No data was used in this paper.

Declarations

Conflict of Interest Not applicable.

References

1. Georgakopoulou, V.E., Lempesis, I.G., Tarantinos, K., Sklapani, P., Trakas, N., Spandidos, D.A.: Atypical pneumonia. Exp. Ther. Med. **28**(5), 424 (2024)
2. Olopade, I.A., Akinola, E.I., Philemon, M.E., Mohammed, I.T., Ajao, S.O., Sangoniyi, S.O., Adeniran, G.A.: Modeling the mathematical transmission of a pneumonia epidemic model with awareness. J. Appl. Sci. Environ. Manage. **28**(2), 403–413 (2024)
3. Paul, J.: Respiratory tract infections. In: Disease Causing Microbes, pp. 99–148. Springer International Publishing, Cham (2024)
4. Yun, K.W.: Community-acquired pneumonia in children: updated perspectives on its etiology, diagnosis, and treatment. Clin. Exp. Pediatr. **67**(2), 80 (2023)
5. Din, A., Li, Y.: Optimizing HIV/AIDS dynamics: stochastic control strategies with education and treatment. Eur. Phys. J. Plus **139**(9), 812 (2024)
6. Sungurlu, S., Balk, R.A.: The role of biomarkers in the diagnosis and management of pneumonia. Clin. Chest Med. **39**(4), 691–701 (2018)
7. Singh, V., Aneja, S.: Pneumonia-management in the developing world. Paediatr. Respir. Rev. **12**(1), 52–59 (2011)

8. Çakar, E., Ta, A., Peters, M., Vinand, E., Waterval-Overbeek, A., Ilic, A., Perdrizet, J.: Economic evaluation of transitioning to the 20-valent pneumococcal conjugate vaccine in the Dutch Paediatric National Immunisation Programme. Infect. Dis. Ther. **14**(3), 527–547 (2025)
9. Alzahrani, S.M.: Statistical methods for the computation and parameter estimation of a fractional SIRC model with Salmonella infection. Heliyon **10**(10), e30885 (2024)
10. Meyer Sauteur, P.M.: Childhood community-acquired pneumonia. Eur. J. Pediatr. **183**(3), 1129–1136 (2024)
11. Abrha, S., Tadesse, E., Atey, T.M., Molla, F., Melkam, W., Masresha, B., Wondimu, A.: Availability and affordability of priority life-saving medicines for under-five children in health facilities of Tigray region, northern Ethiopia. BMC Pregn. Childbirth **18**, 1–9 (2018)
12. Al-arydah, M.T.: Assessing vaccine efficacy for infectious diseases with variable immunity using a mathematical model. Sci. Rep. **14**(1), 18572 (2024)
13. Chapman, T.J., Olarte, L., Dbaibo, G., Houston, A.M., Tamms, G., Lupinacci, R., Banniettis, N.: PCV15, a pneumococcal conjugate vaccine, for the prevention of invasive pneumococcal disease in infants and children. Expert Rev. Vaccines **23**(1), 137–147 (2024)
14. Hethcote, H.W.: The mathematics of infectious diseases. SIAM Rev. **42**(4), 599–653 (2000)
15. Gabrick, E.C., Brugnago, E.L., de Souza, S.L., Iarosz, K.C., Szezech, J.D., Viana, R.L., et al.: Impact of periodic vaccination in SEIRS seasonal model. Chaos Interdiscip. J. Nonlinear Sci. **34**(1), 013137 (2024)
16. Ullah, S.: Investigating a coupled system of Mittag–Leffler type fractional differential equations with coupled integral boundary conditions. J. Math. Techn. Model. **1**(2), 16–28 (2024)
17. Lu, C., Li, L., Shah, K., Abdalla, B., Abdeljawad, T.: Mathematical insights into chaos in fractional-order fishery model. Model. Earth Syst. Environ. **11**(3), 1–17 (2025)
18. Khan, W.A., Zarin, R., Zeb, A., Khan, Y., Khan, A.: Navigating food allergy dynamics via a novel fractional mathematical model for antacid-induced allergies. J. Math. Techn. Model. (2024). https://doi.org/10.56868/jmtm.v1i1.3
19. Ain, Q.T., Din, A., Qiang, X., Kou, Z.: Dynamics for a nonlinear stochastic cholera epidemic model under Lévy noise. Fract. Fraction. **8**(5), 293 (2024)
20. Moghadas, S.M.: Gaining insights into human viral diseases through mathematics. Eur. J. Epidemiol. **21**, 337–342 (2006)
21. Din, A.: Bifurcation analysis of a delayed stochastic HBV epidemic model: cell-to-cell transmission. Chaos Solitons Fract. **181**, 114714 (2024)
22. Wang, L., Xu, R.: Global stability of an SEIR epidemic model with vaccination. Int. J. Biomath. **9**(06), 1650082 (2016)
23. Greenhalgh, D., Lamb, K.E., Robertson, C.: A mathematical model for the spread of Strepotococcus pneumoniae with transmission dependent on serotype. J. Biol. Dyn. **6**(sup1), 72–87 (2012)
24. Wasserman, M., Lucas, A., Jones, D., Wilson, M., Hilton, B., Vyse, A., Farkouh, R.: Dynamic transmission modelling to address infant pneumococcal conjugate vaccine schedule modifications in the UK. Epidemiol. Infect. **146**(14), 1797–1806 (2018)
25. Appel, R.J.C., Siqueira, K.N., Konstantinidis, I., Martins, M.I.M., Joshi, R., Pretto-Giordano, L.G., Fernandes, J.M.D.O.: Comparative transcriptome analysis reveals a serotype-specific immune response in Nile tilapia (Oreochromis niloticus) infected with Streptococcus agalactiae. Front. Immunol. **15**, 1528721 (2025)
26. Sowole, S.O., Sangare, D., Ibrahim, A.A., Paul, I.A.: On the existence, uniqueness, stability of solution and numerical simulations of a mathematical model for measles disease. Int. J. Adv. Math **4**(2019), 84–111 (2019)
27. Doura, K., Meléndez-Morales, J.D., Meyer, G.G., Pérez, L.E.: An S–I–S model of streptococcal disease with a class of beta-hemolytic carriers (Technical Report No. BU-1524-M). Cornell University, Biometrics Unit (1999)
28. Ngari, C.G., Malonza, D.M., Muthuri, G.G.: A model for childhood pneumonia dynamics (2014)
29. Melegaro, A., Gay, N.J., Medley, G.F.: Estimating the transmission parameters of pneumococcal carriage in households. Epidemiol. Infect. **132**(3), 433–441 (2004)
30. Ngari, C.G., Pokhariyal, G.P., Koske, J.K.: Analytical model for childhood pneumonia, a case study of Kenya. Br. J. Math. Comput. Sci. **12**(2), 1–28 (2016)
31. Kizito, M., Tumwiine, J.: A mathematical model of treatment and vaccination interventions of pneumococcal pneumonia infection dynamics. J. Appl. Math. **2018**(1), 2539465 (2018)
32. Teklu, S.W., Mekonnen, T.T.: HIV/AIDS-pneumonia coinfection model with treatment at each infection stage: mathematical analysis and numerical simulation. J. Appl. Math. **2021**(1), 5444605 (2021)
33. Teklu, S.W., Mekonnen, T.T.: HIV/AIDS-pneumonia coinfection model with treatment at each infection stage: mathematical analysis and numerical simulation. J. Appl. Math. **2021**(1), 5444605 (2021)

34. Van den Driessche, P., Watmough, J.: Reproduction numbers and sub-threshold endemic equilibria for compartmental models of disease transmission. Math. Biosci. **180**(1–2), 29–48 (2002)
35. Castillo-Chavez, C., Feng, Z., Huang, W.: On the computation of r(o) and its role on global stability. In: Castillo-Chavez, P.C., Blower, S., Driessche, P., Kirschner, D., Yakubu, A.-A. (eds.) Mathematical Approaches for Emerging and Reemerging Infectious Diseases: An Introduction, p. 229. Springer, Berlin (2001)
36. Safi, M.A.: Global stability analysis of two-stage quarantine-isolation model with Holling type II incidence function. Mathematics **7**(4), 350 (2019)
37. Korobeinikov, A., Wake, G.C.: Lyapunov functions and global stability for SIR, SIRS, and SIS epidemiological models. Appl. Math. Lett. **15**(8), 955–960 (2002)
38. Mickens, R.E.: Dynamic consistency: a fundamental principle for constructing nonstandard finite difference schemes for differential equations. J. Differ. Equ. Appl. **11**(7), 645–653 (2005)
39. Mickens, R.E. (ed.): Nonstandard Finite Difference Models of Differential Equations. World Scientific, Singapore (1993)
40. Eskandari, Z., Avazzadeh, Z., Khoshsiar Ghaziani, R., Li, B.: Dynamics and bifurcations of a discrete-time Lotka–Volterra model using nonstandard finite difference discretization method. Math. Methods Appl. Sci. **48**(7), 7197–7212 (2022)
41. Hoang, M.T., Egbelowo, O.F.: Nonstandard finite difference schemes for solving an SIS epidemic model with standard incidence. Rend. Circolo Mate. Palermo Ser. **2**(69), 753–769 (2020)